

Scalable graphene field-effect sensors for specific protein detection

This article has been downloaded from IOPscience. Please scroll down to see the full text article.

2013 Nanotechnology 24 355502

(<http://iopscience.iop.org/0957-4484/24/35/355502>)

View [the table of contents for this issue](#), or go to the [journal homepage](#) for more

Download details:

IP Address: 128.193.96.87

The article was downloaded on 18/09/2013 at 23:13

Please note that [terms and conditions apply](#).

Scalable graphene field-effect sensors for specific protein detection

Grant Saltzgeber¹, Peter Wojcik¹, Tal Sharf¹, Matthew R Leyden²,
Jenna L Wardini¹, Christopher A Heist³, Adeniyi A Adenuga³,
Vincent T Remcho³ and Ethan D Minot¹

¹ Department of Physics, Oregon State University, Corvallis, OR 97331, USA

² Nanotech Biomachines, Berkeley, CA 94710, USA

³ Department of Chemistry, Oregon State University, Corvallis, OR 97331, USA

E-mail: ethan.minot@oregonstate.edu

Received 15 May 2013

Published 6 August 2013

Online at stacks.iop.org/Nano/24/355502

Abstract

We demonstrate that micron-scale graphene field-effect transistor biosensors can be fabricated in a scalable fashion from large-area chemical vapor deposition derived graphene. We electrically detect the real-time binding and unbinding of a protein biomarker, thrombin, to and from aptamer-coated graphene surfaces. Our sensors have low background noise and high transconductance, comparable to exfoliated graphene devices. The devices are reusable and have a shelf-life greater than one week.

 Online supplementary data available from stacks.iop.org/Nano/24/355502/mmedia

(Some figures may appear in colour only in the online journal)

The detection of protein biomarkers is important for the diagnosis and monitoring of disease. However, the cost and time delays of traditional protein detection techniques are obstacles to the widespread use of biomarker measurements in medicine [1]. Many new alternatives to traditional protein assays are being actively pursued. Among these are nanoscale field-effect transistor (nanoFET) biosensors made from either semiconducting carbon nanotubes (CNTs) [2], silicon nanowires [3] or graphene [4].

NanoFET devices are sensitive to the electrostatic charge of target biomolecules. The electrical resistance of the nanomaterial changes when charged molecules bind in close proximity to the material surface. Graphene, an atomically thin sheet of carbon atoms, is particularly promising as the electric-field-sensitive component of nanoFET biosensors. Graphene FETs (GFETs) on standard substrates exhibit a room temperature carrier mobility in excess of $5000 \text{ cm}^2 \text{ V}^{-1} \text{ s}^{-1}$, significantly better than that for traditional Si FETs [5]. The two-dimensional nature of graphene leads to the additional advantage that all atoms in the transistor channel are electrostatically coupled to the environment. Lastly graphene offers signal-to-noise advantages over its daughter material, CNTs. Devices made

from both materials show baseline noise levels that scale inversely with the square root of the sensing area [6]. Graphene sheets blanket surfaces (unlike individual CNTs), which allows the sensing area to be maximized (noise minimized) for a given amount of on-chip real estate.

A practical limitation of previous GFET biosensors is the use of mechanically exfoliated graphene which is not suitable for scalable fabrication. While this labor intensive mechanical exfoliation technique yields the highest-quality graphene devices, it limits the sensing area to a few square microns, and only allows for one-at-a-time device production [7]. Chemical vapor deposition (CVD) of graphene has emerged as the most promising route to the large-scale production of graphene devices [8]. Sheets of CVD graphene can be produced on the meter scale and transferred to arbitrary substrates [9]. The graphene can then be patterned into devices using standard microfabrication processing. In contrast to exfoliated flakes of graphene, the device size and device location can be easily controlled. With CVD graphene it would be feasible to fabricate hundreds of multiplexed GFET biosensors on a single chip while optimizing the signal-to-noise ratio and the packing density.

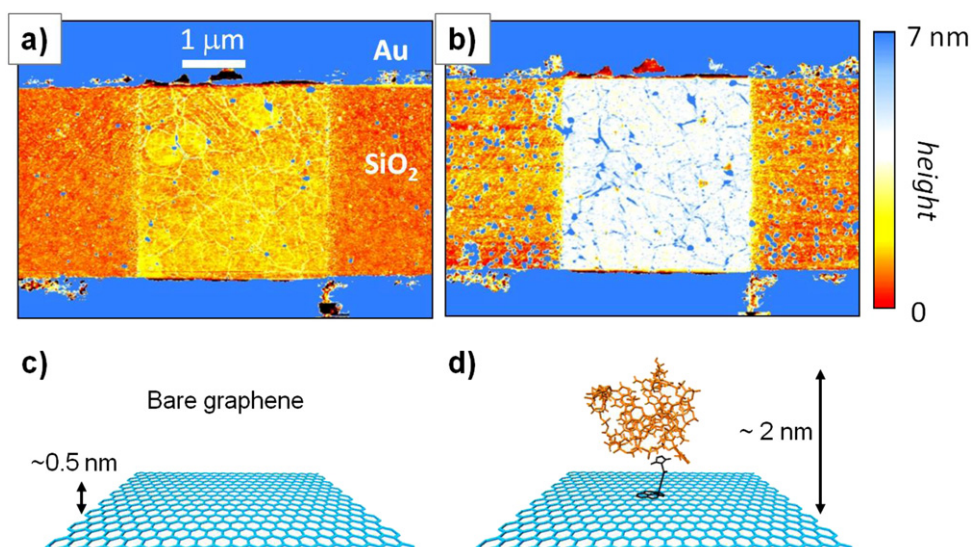


Figure 1. Functionalization of the graphene surface. (a) Atomic force microscopy image showing the bare graphene channel ($3 \times 3 \mu\text{m}^2$) on a SiO_2 substrate. A pair of gold electrodes are seen at the top and bottom of the image. The color scale represents surface height. The bare graphene surface is ~ 0.5 nm above the substrate. (b) Atomic force microscopy image of the same device after treating the surface with PBASE and aptamer. The functionalized graphene surface is ~ 2 nm above the substrate. (c) Illustration of the bare graphene surface, consistent with the first AFM image. (d) Illustration of the functionalized graphene surface showing the molecular structure of PBASE (black) and the molecular structure of the aptamer. The expected size of the PBASE–aptamer construct is consistent with the second AFM image.

Previous work has demonstrated that millimeter-scale GFETs based on CVD graphene can be used for glucose or glutamate sensing [10]. However, this work has not been extended to protein biomarker detection, and the performance of CVD graphene biosensors has yet to be compared with exfoliated graphene. In this work we demonstrate that micron-scale protein-specific GFET biosensors can be constructed using CVD graphene in a scalable fabrication process. We observe minimal variability between the different devices and observe electronic background noise comparable to exfoliated graphene devices. Using ssDNA aptamers for surface functionalization, we demonstrate real-time electronic detection of the protein biomarker thrombin and find excellent agreement with the expected binding kinetics for the aptamer–protein complex. Going beyond previous studies of exfoliated graphene FET protein sensors [11, 12] we also show reversible aptamer–protein binding, demonstrate sensor reusability, and confirm device stability over a one-week time scale.

Graphene was grown on Cu foil using the CVD method [8]. Raman spectra of the graphene on Cu show characteristic properties of single-layer graphene (see supporting information available at stacks.iop.org/Nano/24/355502/mmedia). After growth, polymethyl methacrylate (2% solution of 495 molecular weight PMMA in anisole) was spin-coated on a $1.5 \text{ cm} \times 1.5 \text{ cm}$ square piece of graphene/Cu. The PMMA/graphene/Cu square was then placed into a copper etchant (CE-200 from Transene) for at least 4 h. The PMMA/graphene film was cleaned by soaking in a series of deionized (DI) water baths for a minimum of 12 h, then placed on the device substrate (Si/SiO_2 using 500 nm oxide with pre-defined alignment marks). After

graphene transfer, the PMMA/graphene/ SiO_2/Si chip was dried at 30°C for 4 h. Finally, to remove PMMA we found that open-air heating at 350°C for 4 h gave excellent results.

With graphene on the SiO_2/Si substrate, ribbons of graphene with dimensions $3 \mu\text{m} \times 10 \mu\text{m}$ were patterned using photolithography (bilayer photoresist LOR3A/S1813 from MicroChem) and a dedicated O_2 plasma etcher.

After graphene patterning, we fabricated metal electrodes (1.5 nm Cr/30 nm Au) using standard photolithography, metallization and lift-off by photoresist remover solution. The metal electrodes left a $3 \mu\text{m} \times 3 \mu\text{m}$ area of graphene exposed. This $3 \times 3 \mu\text{m}^2$ graphene surface forms the active sensing area for each GFET biosensor. A total of 24 such GFETs were fabricated on each chip. A small amount of processing residues remained on the graphene surface and we found that removal of these final residues is critical to obtain working devices. For this final cleaning step we followed the work of Ishigami *et al*, annealing the device at 400°C in an Ar/H_2 atmosphere [13]. Figure 1(a) shows a ‘clean’ device. The apparent height of the graphene is approximately 0.5 nm.

To create a functional surface for preferential protein binding, we treated chips with pyrenebutanoic acid succinimidyl ester (PBASE, obtained from Invitrogen) followed by a thrombin-specific DNA-based aptamer (5′-amino C6/GGT TGG TGT GGT TGG-3′, obtained from Integrated DNA Technologies). This aptamer coating is designed to bind specifically to thrombin protein from human plasma (molecular weight 37 kDa, purchased from Sigma Aldrich) with a dissociation constant $K_D \sim 200$ nM [14, 15]. The aptamer immobilization protocol is based on work by Ohno *et al* who immobilized IgE aptamer on mechanically exfoliated graphene [11]. Figure 1(b) shows the device surface after

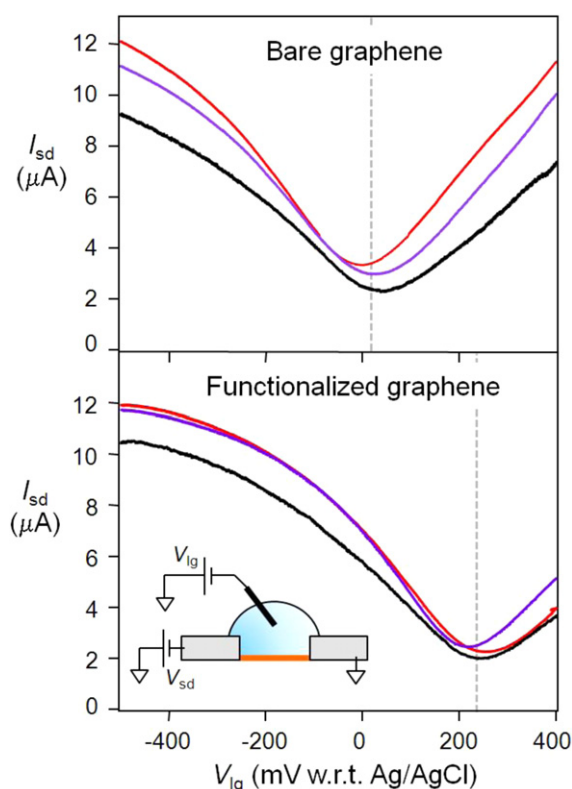


Figure 2. Transistor curves for different GFET devices measured in 5 mM MES buffer solution. The upper panel shows data from three bare graphene devices. For all three devices, the Dirac point (minimum conductance) is close to 0 and the maximum transconductance is $\sim 1.2 \text{ mS V}^{-1}$. The lower panel shows similar data from a set of functionalized graphene devices. The inset shows the circuit diagram corresponding to measurements of $I_{sd}(V_{lg})$.

treatment with PBASE and thrombin aptamer, together with a schematic of the molecular construct.

Analyte solution was delivered to the devices using a home built microfluidic system. Analyte solutions consisted of a 5 mM MES buffer (Debye screening length $\lambda_D \sim 10 \text{ nm}$) mixed with varying amounts of protein. A constant pressure-driven flow of $25 \mu\text{l min}^{-1}$ was used for all experiments. A microfluidic channel was formed above the devices by pressing a polydimethylsiloxane (PDMS) stamp onto the SiO_2/Si chip. The channel dimensions were $100 \mu\text{m}$ height and $200 \mu\text{m}$ width. Before each experiment, the PDMS stamp was cleaned by a 30 min soak in hexane, a 30 min soak in isopropyl alcohol, followed by a 5 min sonication in ethanol, then rinsed with $18.2 \text{ M}\Omega \text{ cm}$ DI H_2O and dried with high purity N_2 . The electrostatic potential of the analyte solution was controlled using a Ag/AgCl reference electrode [16], which was interfaced with the analyte solution downstream of the GFET device. The liquid gate voltage V_{lg} was sourced from a low-noise voltage source (Yokakawa GS200 DC). The source–drain current in the GFET device, I_{sd} , was measured with a low-noise current preamplifier (Stanford Research Systems SR570). All experiments were performed with a source–drain voltage $V_{sd} = 25 \text{ mV}$ (see inset of figure 2). Faradaic currents between the analyte solution

and the GFET device were negligible (more than 100-fold smaller than I_{sd}).

Figure 2, upper panel, shows $I_{sd}(V_{lg})$ for a set of three bare graphene devices. The curves are representative of the typical variability that we observe between different devices. The highest currents correspond to a graphene sheet resistance of $\sim 2 \text{ k}\Omega/\text{sq}$, which is typical for moderately doped single-layer graphene. The location of the Dirac point is $20 \pm 20 \text{ mV}$ w.r.t. Ag/AgCl and the maximum normalized transconductance, $(1/V_{sd}) dI_{sd}/dV_{lg}$, is approximately 1.2 mS V^{-1} .

Figure 2, lower panel, shows $I_{sd}(V_{lg})$ curves for three devices on a chip that underwent the aptamer functionalization protocol. The Dirac point is at $240 \pm 20 \text{ mV}$ w.r.t. Ag/AgCl. The transconductance is not affected by the addition of the functionalization layer. The shift in the Dirac point towards positive liquid gate voltages is consistent with a negatively charged coating on the graphene surface. The DNA-based aptamer has a bare charge of $-15e$, where e is the charge of the electron. This bare charge will be partially screened by condensed ions [17], but the remaining negative charge will produce a potential offset between the graphene and the bulk liquid, thereby shifting the position of the Dirac point to more positive values of V_{lg} .

Before measuring protein interactions with the GFET devices we characterized background noise levels. Following the methods developed by Heller *et al* [6], we measured the power spectral density of current fluctuations at different values of V_{lg} . Using the transduction sensitivity, dI_{sd}/dV_{lg} , we then determined the power spectral density of the effective gate voltage fluctuations, $S_{\text{input}}(f)$. Since $S_{\text{input}}(f)$ is known to scale inversely with frequency, f , and inversely with device area, A , we define an area-independent noise parameter ξ such that $S_{\text{input}}(f) = \xi/Af$. For our devices we find $\xi \approx 0.1 \mu\text{m}^2 \text{ mV}^2$ (see supporting information available at stacks.iop.org/Nano/24/355502/mmedia). Within experimental uncertainty, this area-independent noise parameter is equal to that for GFET biosensors made from exfoliated graphene [6].

Functionalized GFET devices were used to electronically monitor protein–aptamer binding in real time. Thrombin was added to MES buffer at various concentrations ranging from 10 to 300 nM. The signal $I_{sd}(t)$ was recorded while holding V_{lg} constant (figure 3). The V_{lg} operating point was chosen to maximize the transconductance of the device. Between each exposure to thrombin, the GFET was cycled back to MES buffer. As a final test, the device was challenged with a different protein, streptavidin, at a concentration of 100 nM. No signal was observed during exposure to streptavidin.

We interpret changes in $I_{sd}(t)$ as a measure of the surface charge density $\sigma_{\text{bound}}(t)$ on the graphene. Each thrombin protein carries a positive charge at neutral pH [18], and binding/unbinding will contribute to the changes $\Delta\sigma_{\text{bound}}$. These changes in the electrostatic environment result in an effective gate voltage, ΔV_{eff} , proportional to $\Delta\sigma_{\text{bound}}$ [19]. The unique $I_{sd}(V_{lg})$ curve for each device allows one to convert between $I_{sd}(t)$ and $\Delta V_{\text{eff}}(t)$ and thereby quantify bound protein [20, 21]. Figure 3, lower panel, shows $\Delta V_{\text{eff}}(t)$

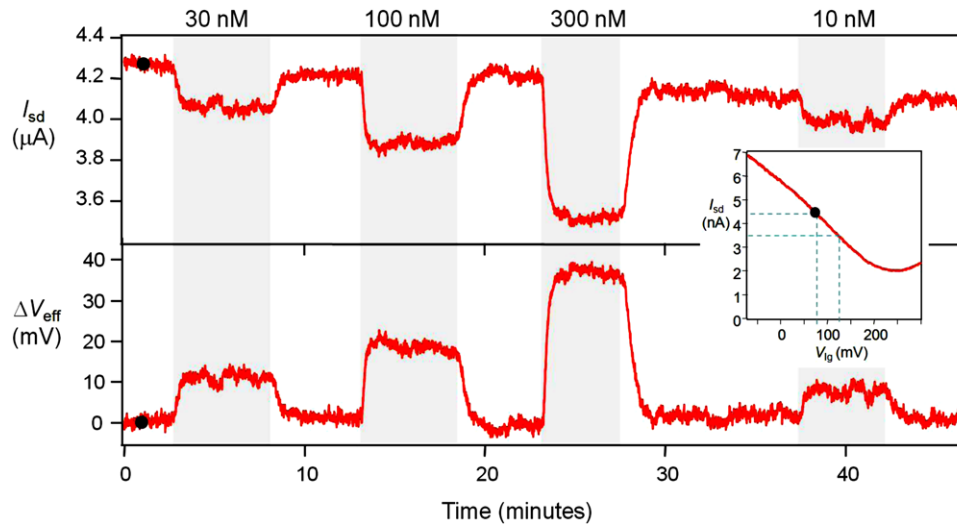


Figure 3. Protein sensing in real time with a GFET device. The four shaded areas (gray) indicate time periods when the device is exposed to thrombin (30 nM, 100 nM, 300 nM and 10 nM respectively). The liquid gate is fixed at $V_{lg} = 75$ mV and a constant flow rate of $25 \mu\text{l min}^{-1}$ was maintained throughout the experiment. Data points were collected every 0.5 s. The upper panel shows raw $I_{sd}(t)$ data. Drops in I_{sd} occur whenever the device is exposed to thrombin. The lower panel shows the calculated effective gate voltage shift $\Delta V_{eff}(t)$. A baseline drift of 0.21 mV min^{-1} was subtracted from this curve. Directly after thrombin is introduced the rate of change of ΔV_{eff} is 21 mV min^{-1} , 67 mV min^{-1} and 106 mV min^{-1} for 30 nM, 100 nM and 300 nM respectively. The inset shows $I_{sd}(V_{lg})$ used to calculate $\Delta V_{eff}(t)$.

calculated from $I_{sd}(t)$. A slowly drifting background has been subtracted from $\Delta V_{eff}(t)$, as discussed below.

We first discuss the rate of thrombin binding on-to and off-of the functionalized surface. For thrombin concentrations below ~ 100 nM the initial rate of thrombin binding to the surface is proportional to the thrombin concentration, indicating a diffusion limited process [22]. These diffusion limited rates are consistent with mass transport modeling of our specific microfluidic geometry [19]. At higher thrombin concentrations, an increase in concentration has less effect on the initial rate of binding. This is consistent with a two-step (diffusion–reaction) process as the binding reaction becomes rate limiting. The unbinding process can be seen when the thrombin solution is exchanged with buffer. Regardless of the preceding thrombin concentration, the decaying signals can be described by one unbinding curve, as expected for a simple one-step release from the surface (see supporting information available at stacks.iop.org/Nano/24/355502/mmedia). In summary, the observed binding kinetics are consistent with theory, and the biosensor can be fully regenerated by a simple rinse.

The equilibrium value ΔV_{eff}^{eqb} , when the on-rate and off-rate balance one another, is a useful parameter for determining the dissociation constant K_D of the binding reaction. From figure 3(b) we know ΔV_{eff}^{eqb} at four different thrombin concentrations. These data points are plotted in figure 4(a). The relationship between ΔV_{eff}^{eqb} and the thrombin concentration is expected to follow a Langmuir isotherm [23]

$$\Delta V_{eff}^{eqb} = \Delta V_{eff}^{max} \times \frac{[\text{thrombin}]}{[\text{thrombin}] + K_D}, \quad (1)$$

where ΔV_{eff}^{max} corresponds to the effective shift in gate voltage when all binding sites are occupied with thrombin.

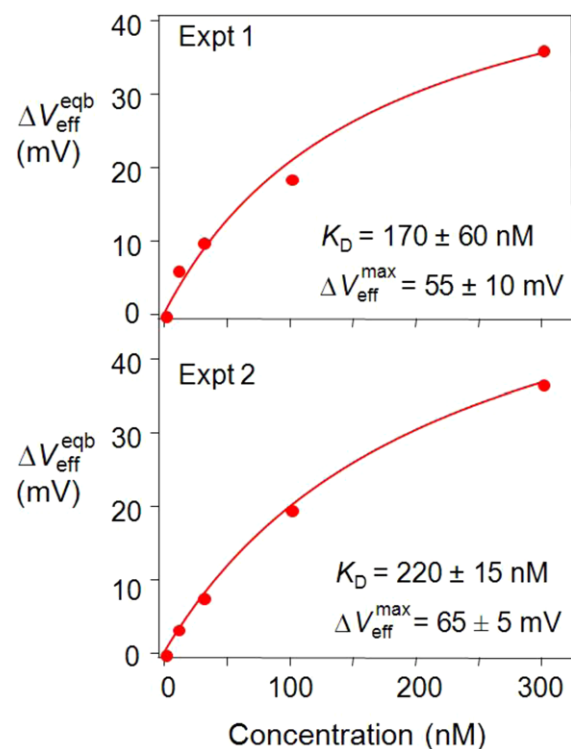


Figure 4. The effective shift in gate voltage, ΔV_{eff}^{eqb} , generated by different thrombin concentrations (red dots). The data are fitted using a Langmuir isotherm (equation (1)). The upper panel shows data from a freshly fabricated device. The lower panel shows data from a different device which had undergone protein binding experiments one week earlier.

Fitting equation (1) to the data points in figure 3(b) yields $K_D = 170 \pm 60$ nM, consistent with previous reports of this aptamer–protein binding reaction [14, 15].

The $I_{sd}(t)$ data in figure 3 show a slow downward drift. We postulate that this changing baseline current is due to pyrene anchors slowly dissociating from the graphene surface. The release of the aptamer coating would shift the Dirac point back towards zero, causing I_{sd} to drop (p-type doping decreased). The measured dI_{sd}/dt corresponds to ΔV_{eff} changing at a rate of 0.21 mV min^{-1} . At this rate, 50% of the aptamer coating would dissociate after approximately 10 h (i.e. the time to reach $\Delta V_{eff} \sim 100 \text{ mV}$). The dissociation rate of the pyrene–graphene bond is an ongoing topic of interest and has led some researchers to design alternative functionalization strategies such as a triple-pyrene anchor molecule [24]. For the experiments described here, a 10 h half-life is more than adequate.

As a final test of the robustness and utility of our CVD-grown GFET biosensor platform, devices were rinsed in DI water, dried with N_2 and stored under ambient conditions. After one week, a GFET sensor was re-interfaced with the microfluidic delivery system and subjected to the same set of measurement protocols. As shown in the bottom panel of figure 4, the bio-recognition PBASE–aptamer element on graphene is reusable, retaining the same biosensing affinity with $K_D \sim 200 \text{ nM}$.

In conclusion, large-area graphene derived from the CVD process can be processed into label-free protein-specific biosensors. This scalable process results in biosensors that are competitive with exfoliated graphene biosensors. Beyond a simple detection of biomarkers, these sensors can also be used to measure binding kinetics. Our results point towards a future where wafer-scale production methods can provide GFET biosensors for a range of biomolecular measurement applications.

Acknowledgments

We thank Joshua Kevek for valuable discussions. This work was supported by the Oregon Nanoscience and Microtechnologies Institute (ONAMI). Device fabrication was partially performed at the MaSC Facility at Oregon State University. Work at the Molecular Foundry was supported by the Office of Science, Office of Basic Energy Sciences, of the US Department of Energy under Contract No. DE-AC02-05CH11231.

References

- [1] Heath J R, Davis M E and Hood L 2009 *Sci. Am.* **300** 44
- [2] Allen B L, Kichambare P D and Star A 2007 *Adv. Mater.* **19** 1439
- [3] Makowski M S and Ivanisevic A 2011 *Small* **7** 1863
- [4] Stine R, Mulvaney S P, Robinson J T, Tamanaha C R and Sheehan P E 2013 *Anal. Chem.* **85** 509
- [5] Schwierz F 2010 *Nature Nanotechnol.* **5** 487
- [6] Heller I, Chatoor S, Mannik J, Zevenbergen M A G, Oostinga J B, Morpurgo A F, Dekker C and Lemay S G 2010 *Nano Lett.* **10** 1563
- [7] Geim A K and Novoselov K S 2007 *Nature Mater.* **6** 183
- [8] Li X S et al 2009 *Science* **324** 1312
- [9] Bae S et al 2010 *Nature Nanotechnol.* **5** 574
- [10] Huang Y X, Dong X C, Shi Y M, Li C M, Li L J and Chen P 2010 *Nanoscale* **2** 1485
- [11] Ohno Y, Maehashi K and Matsumoto K 2010 *J. Am. Chem. Soc.* **132** 18012
- [12] Okamoto S, Ohno Y, Maehashi K, Inoue K and Matsumoto K 2012 *Japan. J. Appl. Phys.* **51** 06FD08
- [13] Ishigami M, Chen J H, Cullen W G, Fuhrer M S and Williams E D 2007 *Nano Lett.* **7** 1643
- [14] Bock L C, Griffin L C, Latham J A, Vermaas E H and Toole J J 1992 *Nature* **355** 564
- [15] Tombelli S, Minunni A and Mascini A 2005 *Biosens. Bioelectron.* **20** 2424
- [16] Minot E D, Janssens A M, Heller I, Heering H A, Dekker C and Lemay S G 2007 *Appl. Phys. Lett.* **91** 093507
- [17] Bockris J O and Reddy A K N 1998 *Modern Electrochemistry I: Ionics* 2nd edn, vol 1 (Berlin: Springer)
- [18] Heuck C C, Schiele U, Horn D, Fronda D and Ritz E 1985 *J. Biol. Chem.* **260** 4598
- [19] Leyden M R, Messinger R J, Schuman C, Sharf T, Remcho V T, Squires T M and Minot E D 2012 *Lab Chip* **12** 954
- [20] Ishikawa F N, Curreli M, Chang H K, Chen P C, Zhang R, Cote R J, Thompson M E and Zhou C W 2009 *ACS Nano* **3** 3969
- [21] Lee B Y, Sung M G, Lee J, Baik K Y, Kwon Y K, Lee M S and Hong S 2011 *ACS Nano* **5** 4373
- [22] Squires T M, Messinger R J and Manalis S R 2008 *Nature Biotechnol.* **26** 417
- [23] Duan X X, Li Y, Rajan N K, Routenberg D A, Modis Y and Reed M A 2012 *Nature Nanotechnol.* **7** 401
- [24] Mann J A, Rodriguez-Lopez J, Abruna H D and Dichtel W R 2011 *J. Am. Chem. Soc.* **133** 17614